Research Square

Preprints are preliminary reports that have not undergone peer review.
They should not be considered conclusive, used to inform clinical practice,
or referenced by the media as validated information.

Evaluation of Wind Energy Potential Using the Rayleigh Distribution for the City of Iriba in Chad

Fia Oung-zetna

fiaoungzetna@gmail.com

University of N'Djamena

Mahamat Alhafis Zenalabidine

University of N'Djamena

Mohamed Ansoumane CAMARA

Gamal Abdel Nasser University of Conakry (UGANC)

Souleymane Soumah

Gamal Abdel Nasser University of Conakry (UGANC)

Noel Djongyang

University of Maroua

Article

Keywords: Wind speed, Rayleigh distribution, Power density, Capacity factor, Cost Energy

Posted Date: August 20th, 2026

DOI: https://doi.org/10.21203/rs.3.rs-10553735/v1

License: This work is licensed under a Creative Commons Attribution 4.0 International License.
Read Full License

Additional Declarations: No competing interests reported.

Evaluation of Wind Energy Potential Using the Rayleigh Distribution for the City of Iriba in Chad

Fia Oung-zetna [a, b*], Mahamat Alhafis Zenalabidine [a], Dr. Mohamed Ansoumane CAMARA[c], Souleymane Soumah[c], Noel Djongyang [b]

[a]Department of Physics, University of N'Djamena, PO Box 1117, N'Djamena, Chad

[b]Department of Physics, University of Maroua, PO Box 58, Maroua, Cameroon

[c]Department of Electrical Engineering, Gamal Abdel Nasser University of Conakry (UGANC), PO Box 1147, Conakry, Guinea

*Corresponding author: Fia Oung-zetna (fiaoungzetna@gmail.com)

Abstract

This study evaluates the technical feasibility and economic profitability of wind energy in Iriba, Chad, to alleviate severe water stress for local populations and livestock. The methodology uses the Rayleigh distribution function to model airflow variability and power density from anemometric data. While the annual average wind speed is 5.56 m/s at ground level, the resource intensifies at a 50-meter hub height, reaching a power density of 414 W/m² in December due to the harmattan. Among three wind turbines evaluated, the EWT DW54-500 model proves most suitable, achieving an efficient annual capacity factor of 39.95%. Financially, this configuration yields a highly competitive Levelized Cost of Energy (LCOE) of 0.031 $/kWh. Ultimately, this work demonstrates that Iriba possesses a clean energy reservoir capable of powering robust water pumping infrastructures, offering a viable techno-economic alternative to fossil fuels for this arid zone.

Keywords: Wind speed, Rayleigh distribution, Power density, Capacity factor, Cost Energy.

1.Introduction

In the context of the ongoing dynamic restructuring of the global energy, the utilization of renewable energy sources has become a strategic necessity for mitigating supply vulnerabilities and reducing the global carbon footprint [1–3]. Among these technological alternatives, the exploitation of wind resources in arid environments offers growing potential, particularly in high-density ecosystems such as the Iriba region in Chad.

This region, characterized by severe drought, faces a structural water shortage that seriously affects residents' livelihoods. The supply of drinking water has traditionally relied on arduous, daily journeys over long distances to fetch water a physical burden disproportionately borne by women. Furthermore, this scarcity of resources is exacerbated by the high water demands resulting from camel herding, a socio-economic pillar of the region. Despite these interrelated constraints, the Iriba region paradoxically benefits from favorable microclimatic factors suitable for the development of wind energy technologies.

Wind measurement data for this specific location reveal an average wind speed of 5.56 m/s at ground level, a promising threshold suggesting that the installation of wind turbines could substantially meet a portion of the community's growing electrical and hydraulic needs. To characterize this resource, the present study relies on the Rayleigh probability density function, a well-established probabilistic approach for modeling

The scientific value of this study lies in its focus on the Iriba region. Indeed, previous wind resource mapping in sub-Saharan Africa often exhibits a smoothing effect, overlooking the complex topographic features and microclimatic peculiarities of remote areas [1, 6, 7]. Consequently, our main hypothesis posits that Iriba's wind potential remains underestimated by global models, and a detailed local study will validate the actual viability of this energy sector.

The framework of this study pursues a dual objective. First, it aims to model wind dynamics in Iriba in detail to quantify its exploitable energy potential. Second, the study evaluates the socioeconomic impacts of such infrastructure, specifically through the optimization of water access via wind-powered pumping systems. By introducing new empirical data into the literature, this study aims to provide clear technical guidelines for the design of future regional energy projects. Ultimately, in alignment with long-term sustainable development goals, it seeks to promote a balanced integration of wind energy into the local energy mix, thereby enhancing the resilience of the community in Iriba.

2. Materials and Methods

2.1. Description of the Study Area and Data Collection

The study area is located in Iriba (15° 07′ N, 22° 15′ E), the capital of the Wadi Fira province in eastern Chad. This site, characterized by a steppe landscape, presents favorable geomorphological conditions for wind energy exploitation, as illustrated by the cartographic overview in Figure 1. To accurately characterize the wind resource, data were extracted from the NASA POWER database and supplemented by records from the National Meteorological Agency of Chad (ANAM). The NASA dataset features a spatial resolution of 0.5×0.5 and an hourly temporal resolution, ensuring a level of precision tailored to energy potential assessments. The physical variables selected for this analysis include wind speeds measured at heights of 10 m and 50 m, as well as the ambient temperature required to compute the local air density. The study relies on a long-term chronological series covering the period from 2000 to 2022 to establish a robust climatological baseline. This is complemented by a detailed analysis of the year 2022 using high-temporal-resolution data to evaluate seasonal and daily variations, enabling the generation of the wind rose diagram.

Data processing, structuring, and initial visualization were performed using Microsoft Excel and LibreOffice Calc. Advanced statistical analysis and modeling were carried out using MATLAB R2021a, which enabled the generation of precise graphical outputs. The wind rose diagram was constructed using WRPLOT software, while the geolocation map was developed using QGIS. Finally, the manuscript drafting was completed using Microsoft Word.

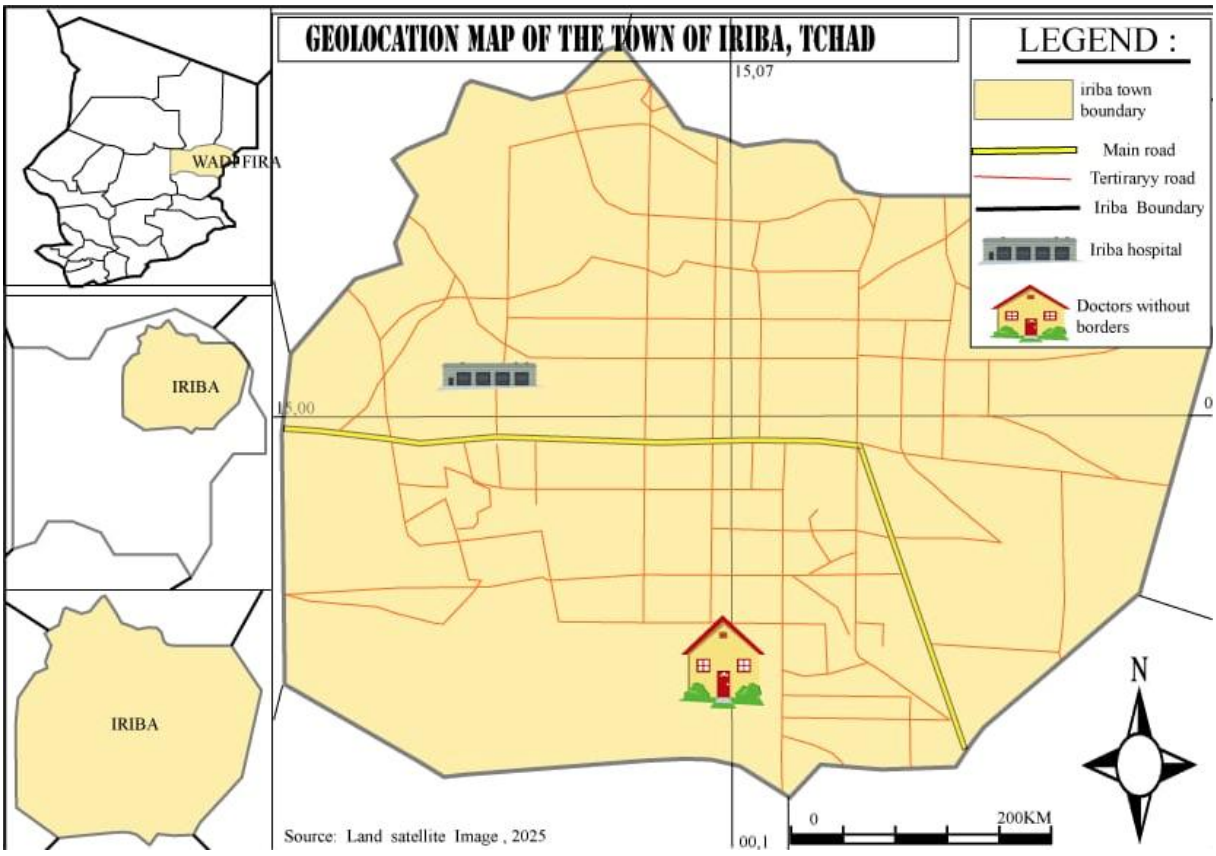


Figure 1: Map of the city of Iriba

2.2. The Rayleigh Distribution function

In contrast to the Weibull framework, which typically demands highly resolved and extensive datasets, the Rayleigh approach provides a reliable alternative for characterizing wind regimes under data-constrained conditions [1–4]. This specific probabilistic model constitutes a particular case of the Weibull function, obtained by fixing the shape parameter (or slope) to a constant value of k = 2. Owing to this mathematical simplification, it serves as a highly practical and widely adopted tool for preliminary wind resource evaluations.

Under this formulation, the systemic mean wind speed Vm is intrinsically coupled to the scale parameter c through the core Gamma (Γ) function, as defined by the following expression:

$$V_m = c.\Gamma\left(1+\frac{1}{k}\right) \quad (1)$$

where:

- Vm: the average velocity;
- c: the scale factor;
- k: the shape factor.

Setting k = 2 for the Rayleigh distribution, equation (1) becomes:

$$V_m = c.\Gamma\left(\frac{3}{2}\right) \quad (2)$$

Since $\Gamma(3/2) = \frac{\sqrt{\pi}}{2}$, we can express the scale factor c directly in terms of the average wind speed[5, 6]:

$$c = \frac{2V_m}{\sqrt{\pi}} \quad (3)$$

Substituting into the Weibull distribution formula yields the Rayleigh distribution [6, 7]:

$$f(V) = \frac{\pi V}{V_m^2} exp\left(-\frac{\pi}{4}\left(\frac{V}{V_m}\right)^2\right) \quad (4)$$

2.3. Analysis of wind speed based on elevation

To accurately assess wind potential at the hub height of modern wind turbines, vertical projection of anemometric data is essential, particularly when primary measurements are limited to a single reference altitude [7, 8]. This assessment of vertical wind shear is fundamental to wind energy meteorology, as the dynamics of the boundary layer cause significant velocity gradients between different atmospheric layers. By extrapolating near-surface data to higher altitudes typically using mathematical formulas such as the power law or the logarithmic profile researchers can comprehensively map the available kinetic energy. Consequently, this reconstruction of the vertical profile reduces uncertainties in resource estimation, enabling optimal aerodynamic design and maximizing the long-term energy yield of future wind infrastructure [10].

2.3.1. Formulation of the Modified Power Law

The estimation of the vertical wind shear profile within this modified model is based on a power law relationship for projecting the velocity field onto the various layers of the atmosphere. Mathematically, the wind speed V_2 calculated at the target operational altitude Z_2 is derived from the initial speed measurement V_1 recorded at the reference altitude Z_1 using the following formula [11, 12]:

$$\mathbf{V_2 = V_1\left(\frac{Z_2}{Z_1}\right)^{\alpha}} \quad (\mathbf{5})$$

where:

- α: the roughness coefficient;

- Z_1: the wind speed at a height of 10 m;

- Z_2: the wind speed at height Z;

- Z: the altitude.

The roughness coefficient is defined by:

$$\alpha = 0.37 - 0.088ln(V_1) \tag{6}$$

Furthermore, the basic parameter of the Rayleigh scale which was initially calculated based on a standard reference height of 10 m must be scaled to reflect the wind conditions at the projected height of the turbine. This altitudinal projection of the statistical parameters is achieved by applying the coupled analytical expressions described in detail in [8, 13]:

$$c_z = c_1 \left(\frac{z}{10}\right)^{\alpha} \tag{7}$$

- c_z: The scale factor at height z;

2.4. Energy Efficiency of the Wind Turbine

2.4.1. Assessment of wind power density

Wind power density is a key metric for determining the inherent quality and energy sustainability of an aerodynamic site. From a physical standpoint, this factor quantifies the flow of kinetic energy passing perpendicularly through a cross-sectional unit covered by the rotor blades. Based on atmospheric parameters, the available power density can be expressed by the following analytical equation:

$$P = \frac{1}{2}\rho v^3 \tag{8}$$

2.4.2. Estimation of usable output power

Considering both the highly variable wind speed and the operating limits of the wind turbine which are determined by the cut-in speed v_1, rated speed vn, and cut-out speed vs the net power that can be generated is expressed by the following equation [12, 15–17]:

$$< P_u >= \frac{1}{2}\rho S < v_u^3 > \tag{9}$$

where:

- ρ: the density ρ = 1.225 kg/m³
- S: the area swept by the blades;

2.4.3. Formulation of the useful power density

The velocity variable v_u is determined based on the Rayleigh distribution profile, which is strictly bounded by the system's operating limits. The lower limit corresponds to the activation

threshold; therefore, any wind speed below v_1 is excluded from the evaluation. Within the second operating mode, once the rated speed v_n is reached, subsequent increases in wind speed do not alter the rotor's mechanical rotational speed. Finally, upon reaching the stall speed v_s, an automatic braking mechanism is activated, meaning that any higher wind speeds are completely omitted from the calculation of v_u. Consequently, the mathematical model for power output density is defined by the following formula [18–20]:

$$< P_u >= \begin{cases} 0 & for \quad v < v_i \\ \frac{1}{2}\rho < v^3 > & for \quad v_i \le v \le v_n \\ \frac{1}{2}\rho v_n^2 & for \quad v_n \le v \le v_s \\ 0 & for \quad v > v_s \end{cases} \tag{10}$$

2.4.3. Wind Turbine Output Power and Efficiency

Every wind energy conversion system is designed to maximize its operational efficiency within specified limits of rated power and wind speed. Consequently, once the scale and shape parameters of the Rayleigh distribution are determined, the performance of a wind turbine at a specific location can be easily evaluated using the average output power and the efficiency coefficient. In this study, the electrical output power of the selected wind turbine model is simulated using the following formula [21–23]:

$$P_e = \begin{cases} 0 & (v < v_d) \\ P_n \dfrac{v^2 - v_d^2}{v_n^2 - v_s^2} & (v_d \le v \le v_n) \\ P_{eR} & (v_n \le v \le v_c) \\ 0 & (v_c < v) \end{cases} \tag{11}$$

Where:

- P_n: rated power
- v_d: the wind turbine's starting speed;
- v_n: rated speed;

v_c: cut-off speed

2.4.4. Evaluation of Generated Electrical Power

The electrical power generated by a wind energy conversion system is strictly governed by the technical specifications set by the manufacturer. Specifically, the relationship between the actual useful power and the nominal power specified by the manufacturer is expressed mathematically by the following equation [24–26]:

$$P_u = C_f P_n \tag{12}$$

Starring:

$$C_f = \frac{e^{-\left(\frac{V_d}{c}\right)^2} - e^{-\left(\frac{V_n}{c}\right)^2}}{\left(\frac{V_n}{c}\right)^2 - \left(\frac{V_d}{c}\right)^2} - e^{-\left(\frac{V_c}{c}\right)^2} \quad (13)$$

Thus, the output power of a wind turbine can be expressed as [27][28]:

$$P_u = \left(\frac{e^{-\left(\frac{V_d}{c}\right)^2} - e^{-\left(\frac{V_n}{c}\right)^2}}{\left(\frac{V_n}{c}\right)^2 - \left(\frac{V_d}{c}\right)^2} - e^{-\left(\frac{V_c}{c}\right)^2} \right) P_u \quad (14)$$

where:

- Cf: the capacity factor, which plays a very important role in the assessment of a wind farm site;
- P_n: the rated power specified by the turbine manufacturer;

2.4.5. Efficiency Coefficient and Overall Energy Efficiency

The efficiency coefficient can be calculated using the parameters of the Rayleigh distribution in combination with the specific operating speeds specified by the manufacturer [29, 30]. Typically, the nominal power Pn is a fixed specification provided by the manufacturer. By determining the actual net output power, the total electrical energy generated by the system over a specified time period can be quantified. Specifically, based on the average net electrical output power (Pe), the cumulative energy yield (Ee) expected over a time period T (in hours) is expressed as:

$$E_e = P_u T = Cf.P_n.T \quad (15)$$

where:

- Pe: electrical power produced;
- Ee: total energy generated;
- T: period.

2.5. Economic Evaluation of Wind Energy

Estimating the cumulative costs over the entire lifetime of a wind energy conversion system is essential for determining its financial and economic viability [31, 32]. Total capital requirements are largely influenced by the rated power and the specific technology provided by the manufacturer. Although modern wind turbine designs minimize operating and maintenance costs during the initial stages, these costs inevitably rise as the facility ages. Furthermore, the final cost of energy depends on the structural infrastructure, the availability of local wind resources, the technical lifespan of the wind turbine, and the selected discount rate.

Among the various economic evaluation techniques available, this study uses the cost-per-kilowatt-hour metric. The financial analysis is structured around the present value of energy alongside the net present value. Consequently, the unit cost per kWh is mathematically defined by the following expression [33, 34]:

$$CPU = \frac{PVC}{E_e} \tag{16}$$

where:

- Ee: energy output over the lifetime of a wind turbine;
- PVC: present value cost

2.5.1. Assumptions regarding the present value of costs (PVC)

The present value of costs (PVC) is calculated using Equation (16), based on the following underlying economic and technical assumptions [35–37]:

$$PVC = I + C_{OMR}\left(\frac{1+i}{r-i}\right)\left(1-\left(\frac{1+i}{1+r}\right)^{n}\right) - S\left(\frac{1+i}{r-i}\right)^{n} \tag{17}$$

where:

- I: The initial investment rate;
- COMR: Annual operating, maintenance, and repair costs;
- S: The residual value;
- i: The inflation rate;
- r: The discount rate;
- n: The useful life

2.5.2. Operational and Economic Parameters

To perform the numerical simulation using the net present value (NPV) method, the evaluation includes the following specific economic and technical criteria:

- The service life of the wind turbine installation is assumed to be n = 20 years.
- The nominal interest rate (r) and local inflation rate (i) are set at 8% and 9%, respectively.
- Current operating, repair, and maintenance costs (ORMC) are projected to equal 25% of the asset's annual cost (defined as the initial purchase price divided by the lifespan) [38].

The detailed breakdown of specific investment expenditures and mean specific costs relative to the rated capacity of the turbine models is consolidated in Table 1.

Table 1: Technical and financial specifications of the selected wind turbines relative to their rated capacity [37, 38]

Turbine power in (kW)	Specific cost (US$/kW)	Average unit cost
10 à 20	2200 à 2900	2550
20 à 200	1500 à 2300	1900
Supérieure à 200	1000 à 1600	1300

3. Results and Discussion

3.1. Results of the statistical analysis of the data

Table 2 presents the results of the analysis of data from NASA and ANAM. The statistical evaluation of the predictive model against experimental measurements (Mi) over the 12-month period demonstrates robust overall simulation capability, although localized temporal discrepancies remain. The overall performance is summarized in the final summary row (MEAN / TOTAL), showing an overall root mean square error (RMSE) of 0.4099, a relative RMSE (RRMSE) of 8.06%, a coefficient of determination (R^2) of 0.8685, and a total chi-square deviance of 0.3984.

On a monthly scale, the model demonstrates exceptional accuracy during the spring and summer seasons. Maximum predictive accuracy is achieved in July (g), where the model records its lowest absolute error (RMSE = 0.0200; RRMSE = 0.52) and a nearly perfect correlation (R^2 = 0.9998). A similar trend of high accuracy is observed in April (d) (RMSE = 0.0700, R^2 = 0.9913) and in December (l) (RMSE = 0.0300, R^2 = 0.9996).

Conversely, a localized breakdown in the model's reliability occurs in October (j), which represents the main statistical anomaly in the dataset. During this month, the error metrics peak critically (RMSE = 0.9400, RRMSE = 16.91) and result in a severe negative deviation of the local coefficient of determination (R^2 = -3.5640).

Table 2: Values of the various calculated errors

Month	RMSE	RRMSE (%)	R^2	χ^2
a. Jan	0.2800	4.46 %	0.9417	0.0120
b. Feb	0.5800	9.68 %	0.5556	0.0512
c. Mar	0.5900	10.35 %	-0.0348	0.0553
d. Apr	0.0700	1.19 %	0.9913	0.0008
e. May	0.1800	3.54 %	-35.0000	0.0061
f. Jun	0.1600	3.84 %	0.9716	0.0064
g. Jul	0.0200	0.52 %	0.9998	0.0001
h. Aug	0.2900	8.73 %	0.9740	0.0278
i. Sep	0.2300	7.23 %	0.9859	0.0179
j. Oct	0.9400	16.91 %	-3.5640	0.1913
k. Nov	0.4100	7.71 %	-3.2025	0.0293
l. Dec	0.0300	0.45 %	0.9996	0.0001
MEAN / TOTAL	0.4099	8.06 %	0.8685	0.3984

3.1.1. Discussion and Analysis of Error Performance

3.1.2. Overall Model Validation

According to standard statistical literature (particularly classification criteria for simulation models), an RRMSE of less than 10% indicates an excellent model. Similarly, according to the criteria of Moriasi et al., [44] an $R^2 > 0.80$ indicates a very strong statistical fit between the actual measurements and the simulations. With an overall RRMSE of 8.06%, the predictive framework developed here fully meets the most stringent validation criteria. This validation is reinforced by the overall R^2 score of 0.8685, indicating that 86.85% of the total variance in the measured data (Mi) is successfully explained by the simulated values (Si).

Furthermore, the cumulative chi-square value (0.3984) is exceptionally low. In a standard chi-square goodness-of-fit test with 11 degrees of freedom (n = N - 1), this value lies well below the critical threshold, confirming that there is no statistically significant difference between the observed distribution and the simulated distribution.

3.1.3. Analysis of Anomalies and Negative R^2 Values

A notable mathematical feature of the monthly decomposition is the presence of negative R^2 values, specifically in March (-0.0348), May (-35.0000), October (-3.5640), and November (-3.2025).

In a purely local context (monthly, point-by-point), a negative R2 does not mean that the overall model is flawed. Mathematically, this occurs when the individual error for the month $\sum(Si - Mi)^2$exceeds the variance relative to the overall annual average of the simulations $\sum\left(Mi - \overline{S}\right)^2$.

- In May (e), the massive drop to -35.0000 is a mathematical artifact: during this month, the measured value (5.09) is extremely close to the overall series mean ($\overline{S} \approx 5.31$). This reduces the denominator of the R^2 formula to a value close to zero, artificially amplifying a simulation error that is, however, minor in absolute terms (RMSE = 0.1800).
- In October (j), however, the negative R^2 reflects a real physical or algorithmic divergence. The model has clearly overestimated or underestimated an abrupt seasonal transition, failing to capture the discontinuity in the measured phenomenon.

3.2. Monthly Variation in Wind Speed

An analysis of the data collected at 10 m and 50 m above ground level (Figures 2 and 3) provides a clear picture of Iriba's climate. It reveals a site where the wind follows a distinct seasonal pattern, offering real opportunities but also presenting some technical challenges. Looking at Figure 2, we are immediately immersed in Chad's climate cycle. It all begins in November, when the wind gains strength, reaching its peak during the winter (December through February). With peaks of 6.67 m/s, this period is a real boon for wind turbine productivity. This is when the site operates at full capacity. After a slight lull in April and May, a more pronounced slowdown is observed between June and October. The lowest point occurs in September, with an average of 2.95 m/s. This dip is a crucial factor to anticipate: it could lead to a drop in output, making the use of a backup power source essential to ensure continuous service.

Figure 3 offers a very encouraging outlook. While it follows the same curve as the first, the values are significantly higher due to the increase in altitude. The conclusion is clear: the higher

you go, the stronger the wind becomes. At 50 meters, the maximum climbs to 8.96 m/s, and even at the lowest point of the year, we remain at 4.45 m/s. This is a strong argument in favor of large wind turbines. By harnessing winds at higher altitudes, we not only optimize overall energy production but also offset some of the weaker surface winds during the off-season.
Figure 4, in turn, shows month-to-month variations over the years, with wind speeds exhibiting significant fluctuations toward the end and beginning of each year, reflecting the prevalence of the harmattan. The dip observed between August and September corresponds to the rainy season, when relative humidity reaches its peak. This drop in wind speed impacts energy production and requires a backup power source.

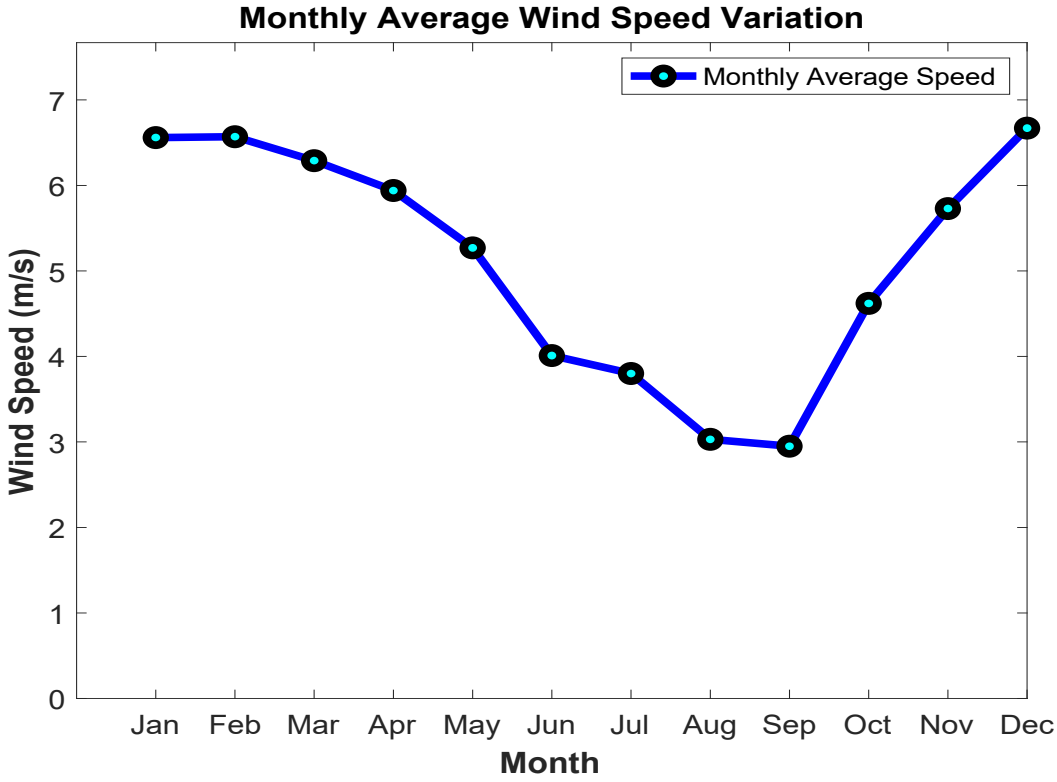


Figure 2: Wind speed trends in the city of Iriba at a height of 10 meters above ground level

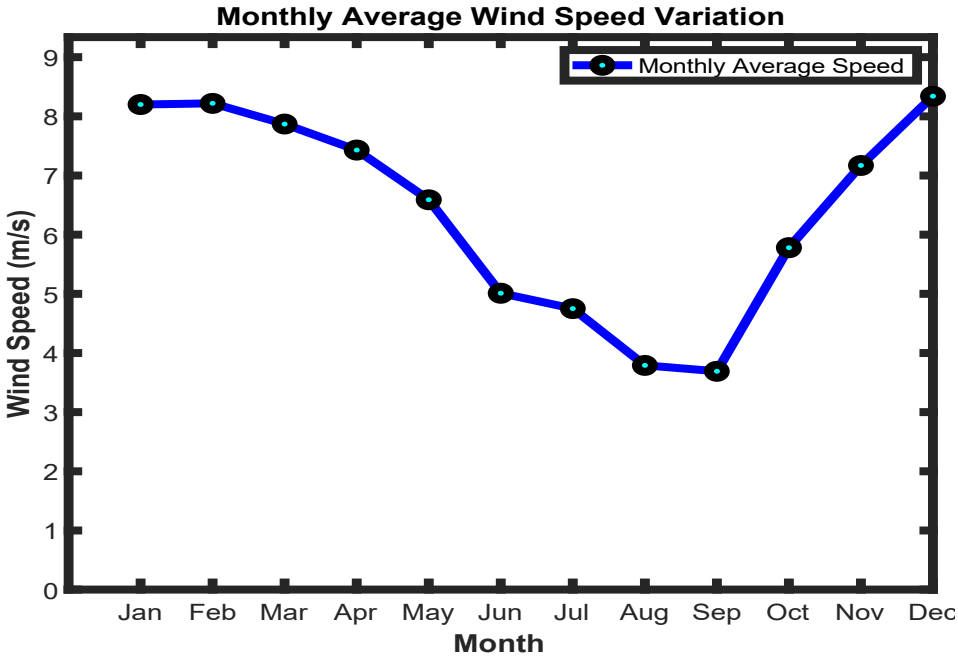


Figure 3: Monthly wind speeds at 50 meters above ground level

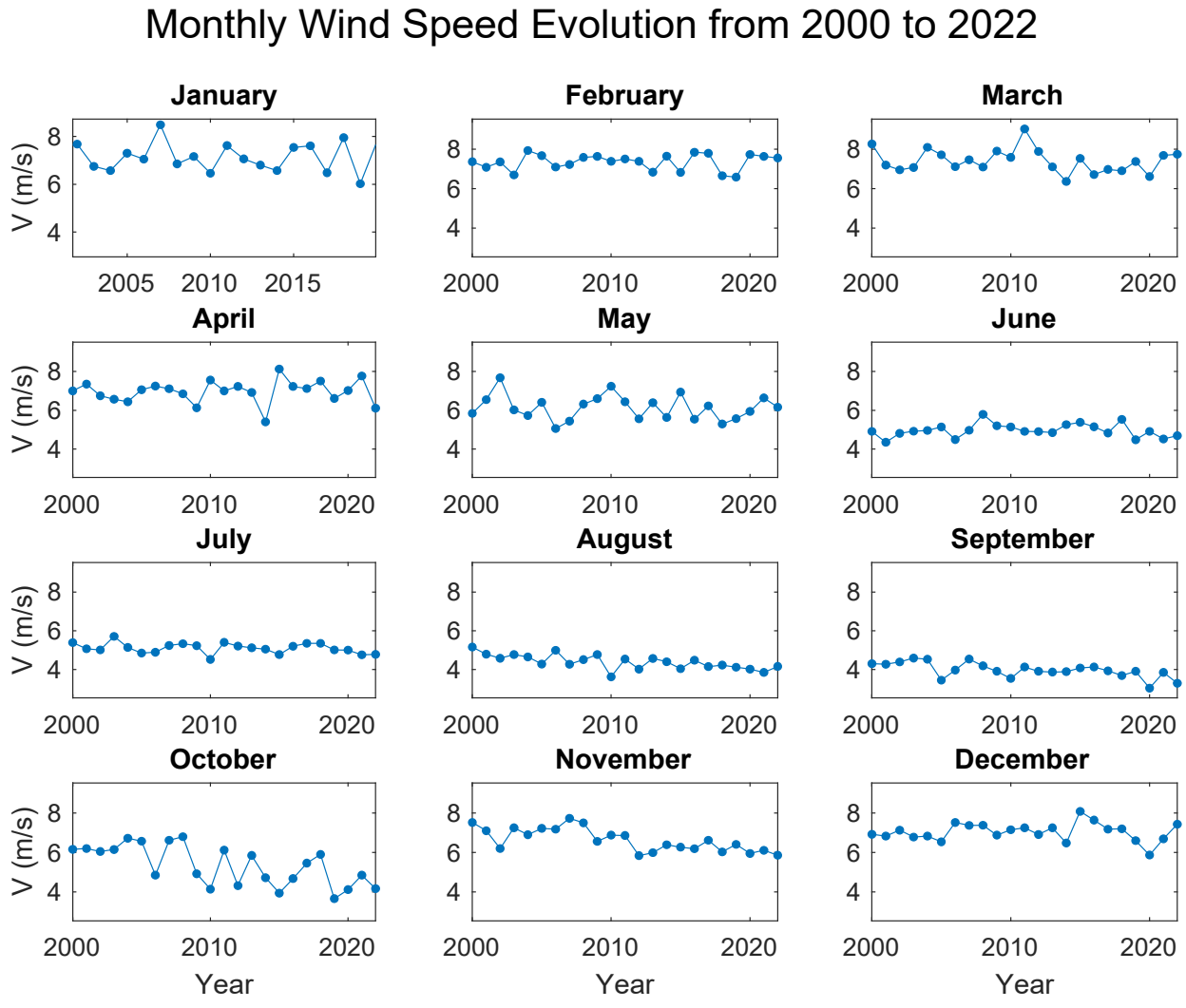


Figure 4: Interannual fluctuations of monthly mean wind velocities.

3.3. Analysis of Wind Power Density in Iriba

Figure 5 shows a marked seasonal fluctuation in the power available at 10 m above ground level in Iriba, revealing a clear contrast between different times of the year.

It is observed that wind potential peaks during the dry season, particularly between November and April. December stands out as the most energy-rich month, with a power density exceeding 180 W/m². This performance is explained by the predominant influence of the harmattan, the northeasterly winds that blow steadily and regularly over the region during this period.

Conversely, a significant decline begins in May, reaching its lowest point between July and September. The annual minimum is recorded in September, with a value dropping to around 16 W/m². This decline corresponds to the transition to the rainy season, when wind patterns change direction and lose intensity.

From a practical standpoint, this distribution is particularly advantageous. Power output is at its peak precisely when the need for hydraulic pumping is most critical (at the height of the dry season). Although wind speeds decline in the middle of the year, the high values recorded over a period of more than six months confirm that Iriba is a favorable site for wind power generation. To ensure a stable energy supply year-round, combining wind power with solar power (which is often abundant when the wind dies down) would be a robust solution.

Moving to a height of 50 meters, as shown in Figure 6, radically changes the perspective on Iriba's wind resource. This elevation allows us to move out of the ground friction zone to capture much more stable and energetic winds, representative of what an industrial-scale wind turbine could harness. The first observation is the dramatic increase in power density. While values at ground level were modest, they reach peaks here, particularly in December with a high of 414.09 W/m². Between November and March, the resource remains consistently above the 300 W/m² threshold, which ranks the Iriba site among the areas with high energy potential in the region.

We see the same seasonal patterns as in ground-based measurements, but with greater resilience. The influence of the Harmattan is fully evident here. The available power is more than double that measured at ground level, offering a real opportunity for large-scale electricity generation. Although the site is experiencing its annual low (around 48 to 52 W/m²), these values remain technically viable for small-scale applications, demonstrating that altitude partially compensates for the seasonal weakness of the winds.

These results hold concrete promise because, with a power density often exceeding 400 W/m² during the high season, the installation of modern wind turbines is not only technically feasible but also economically promising. This power available at 50 meters could transform the local economy, moving from simple water pumping to true rural electrification capable of supporting agricultural and pastoral activities year-round.

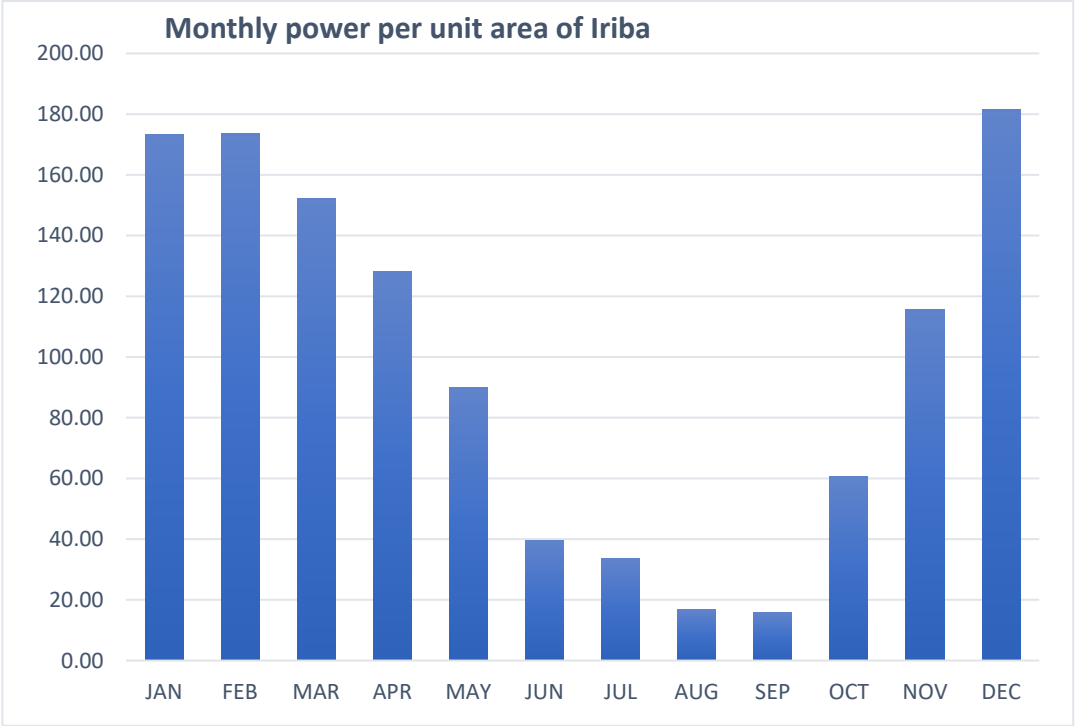


Figure 5: Wind power density distribution simulated at a height of 10 m.

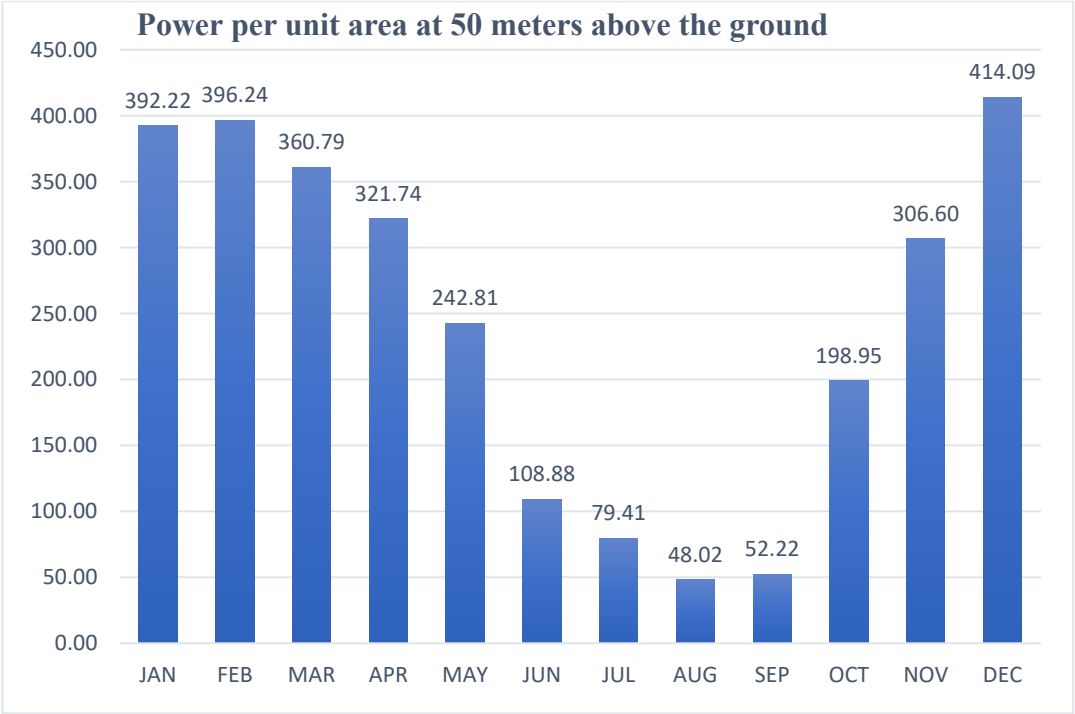


Figure 6 : Wind power density at 50 m hub height

3.3.1. Analysis of the Statistical Distribution of Wind Speed

Calculating the parameter c using the maximum likelihood method with k=2 yields c=5.39 m/s. Analysis of Figure 7 shows that the wind speed range is quite broad, indicating that the area is suitable for wind turbine installations. The most frequent wind speed is around 3 to 4 m/s: this is the range where the histogram is highest and where the red theoretical curve reaches

its peak. Between approximately 2 and 8 m/s, the model fits the data fairly well, suggesting that the Rayleigh distribution accurately describes the primary behavior of the wind. When speeds exceed about 8 m/s, the probability gradually decreases: strong winds do occur but are significantly less frequent. The distribution also has a tail, with possible occurrences up to about 12–16 m/s, but these are rare.

Figure 8 shows the various monthly wind speed distribution curves. It can be seen that the probability density ranges from 0.1 to 0.26 throughout the year. From December through April, the wind speed range remains wide, indicating a period favorable for wind power generation. The months of August and September show peaked distributions with narrow bandwidths, indicating a season of low wind energy production. This distribution highlights the most favorable and least favorable months.

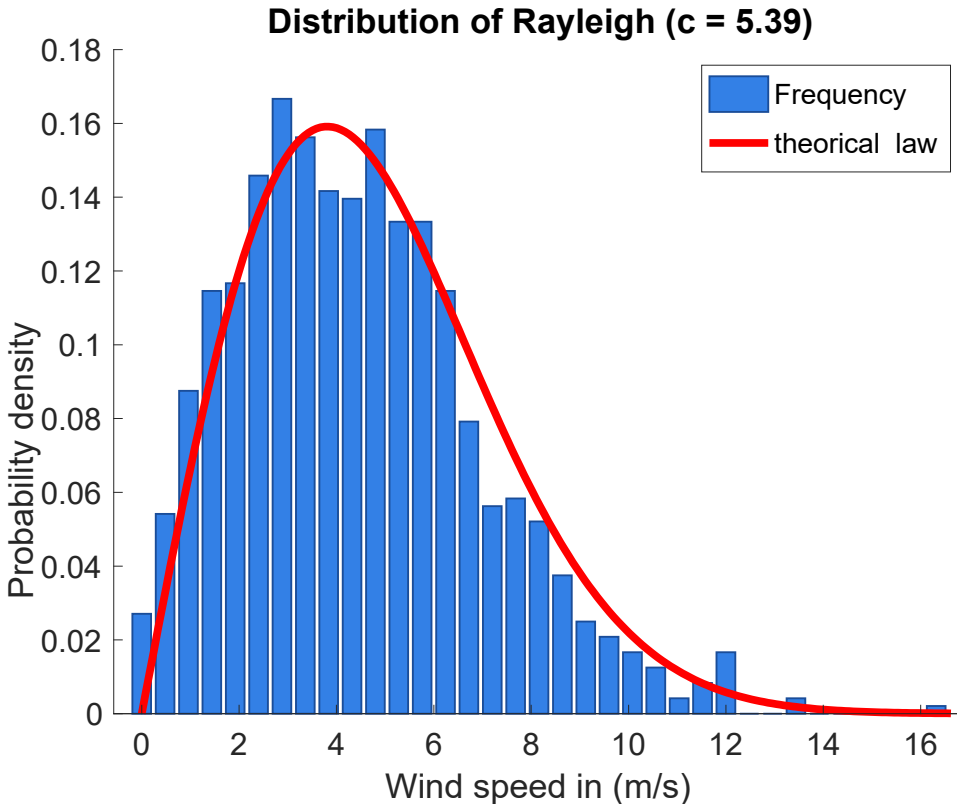


Figure 7: Rayleigh frequency distribution characterizing the Iriba region.

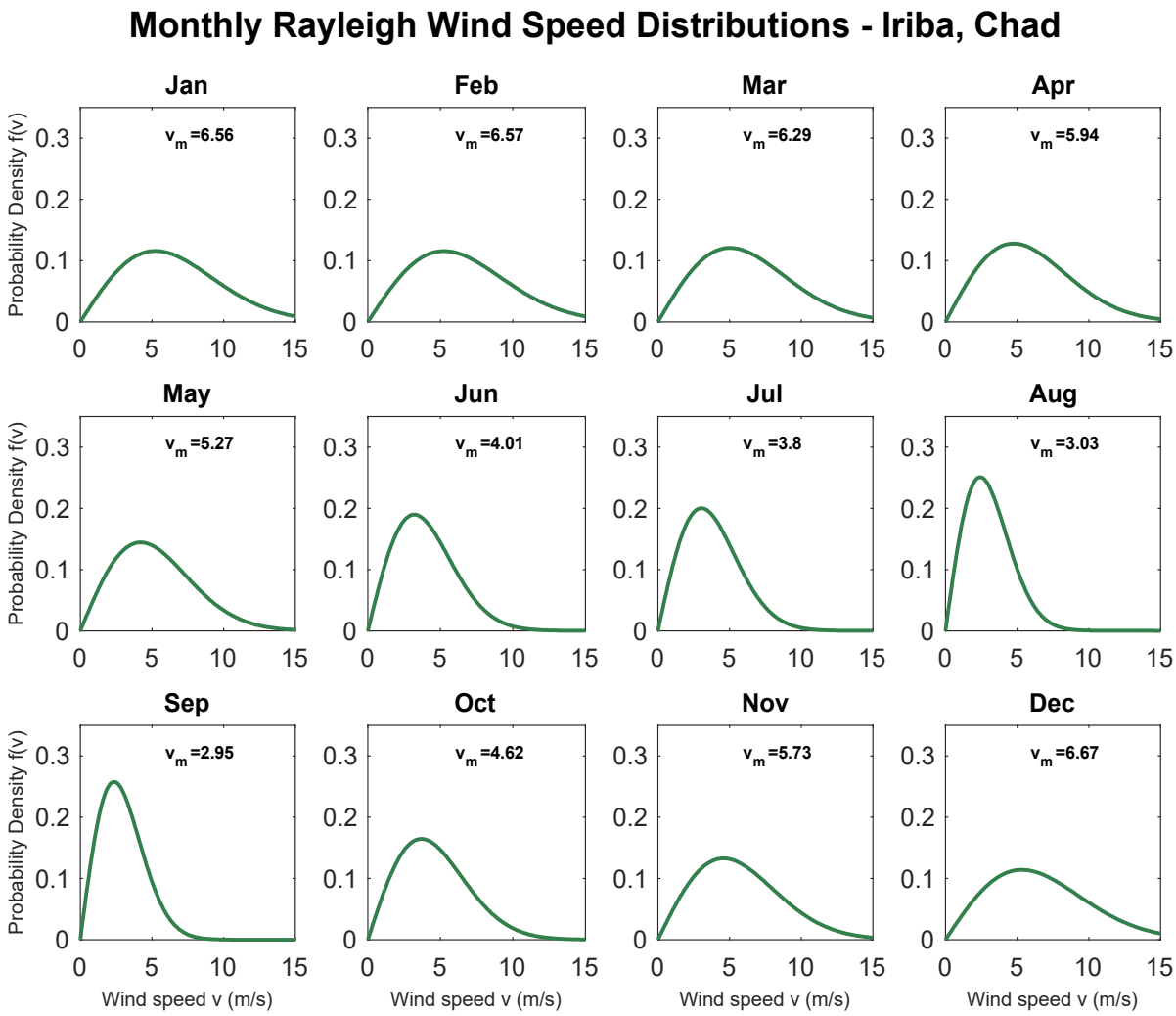


Figure 8: Monthly Rayleigh wind speed probability density distributions for the site of Iriba

3.3.2 The site's wind rose

Analysis of the wind rose diagram in Figure 9 for the Iriba site highlights the directional distribution of wind flows and their speed ranges. It can be observed that the prevailing wind for speeds between 5.70 and 8.80 m/s comes from the northeast. The frequencies associated with this sector vary between approximately 29.5% and 36.9%, indicating a relatively high occurrence of these wind conditions. Furthermore, a second significant regime corresponds to speeds between 8.80 and 11.10 m/s. For this range, the winds also come from several directions, with frequencies ranging from approximately 14.8% to 29.5% (values that vary depending on the direction within the diagram). Thus, these results specify which directions are most favorable for winds of medium to high speed. They complement the analysis of probability densities by providing essential information for the planning and orientation of wind turbine placement at the Iriba site.

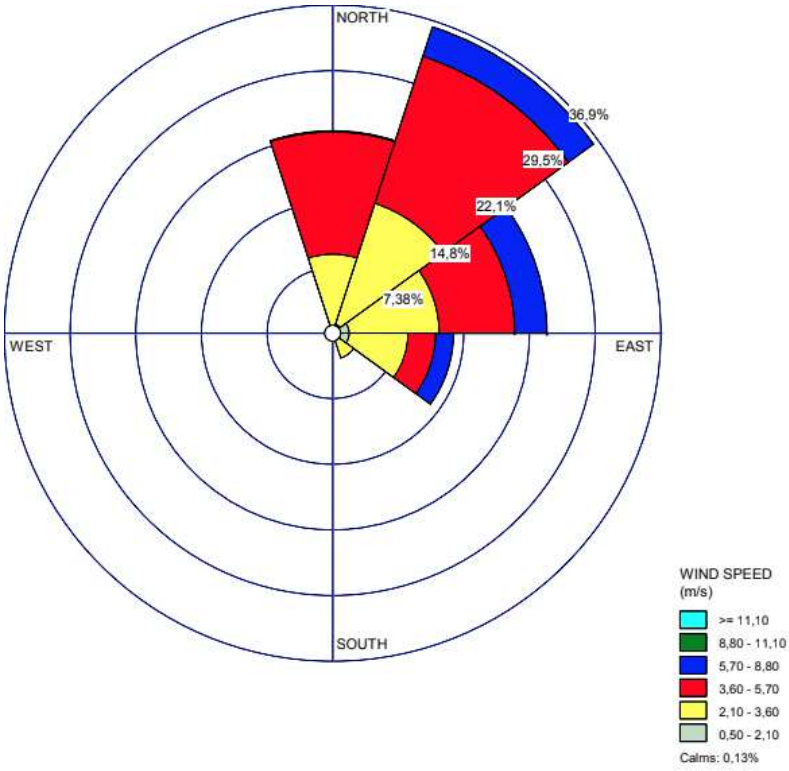


Figure 9: Iriba's wind rose diagram

3.4. Performance Evaluation and Energy Yield of Selected Wind Turbines

The selection of the technology portfolio shown in Table 5—whose performance curves are presented in Figure 10—consists of the EWT DW54-500, Antaris 30 kW, and Vestas V52 models. This selection was made to compare distinct aerodynamic designs with the meteorological conditions in Iriba. The primary objective is to evaluate the actual performance of each turbine based on local wind speed and direction data, in order to determine which technical profile best optimizes the load factor in this Saharan environment.

The EWT DW54-500, with its oversized rotor, is being tested for its ability to maximize energy capture in moderate winds, while the Antaris 30 kW serves as a benchmark for responsiveness to low wind speeds, which are essential for continuous hydraulic pumping. At the same time, the Vestas V52 allows for the analysis of a high-power turbine's performance under the sustained wind conditions of eastern Chad. This comparative analysis, based on your in-situ measurements, aims to identify the turbine offering the best technical and economic performance, thereby ensuring that the final solution is perfectly calibrated to sustainably address the region's water stress and energy needs.

Table 3: Wind turbines for various applications at the Iriba site

Model	Rated power	Start-up speed	Rated speed	Shutdown speed	Rotor diameter	Mast height
EWT DW54-500	500kW	2,5 m/s	10 m/s	25 m/s	54 m	50 m
Antaris 30 kW	30 kW	2,2 m/s	11m/s	20 m/s	12,5 m	50 m
VestasV52	850 kW	4 m/s	15 m/s	25 m/s	52 m	50 m

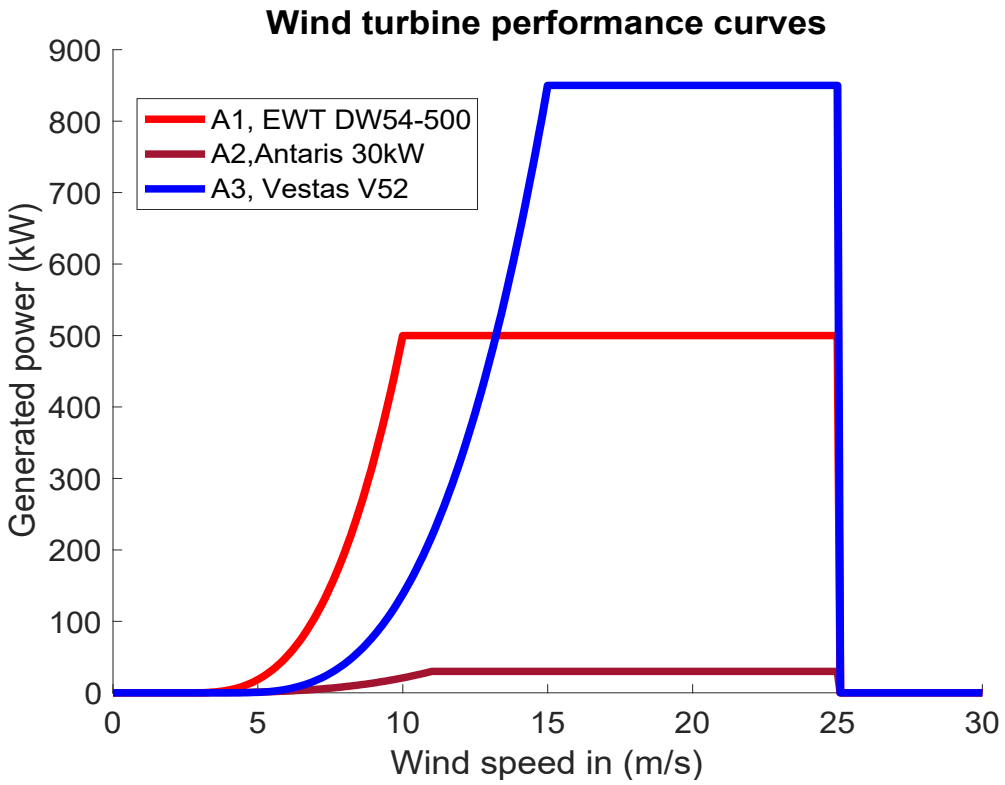


Figure 10: Performance curve of wind turbines

3.4.1. Applications to wind turbines using local data

Analysis of Tables 4, 5, and 6 reveals a marked seasonal pattern: generation increases and the cost per kWh decreases when wind conditions are favorable, while the opposite occurs during calm periods.

Table 4: Monthly aerodynamic and economic performance of the Antaris 30kW turbine in Iriba

	Month	c (m/s)	Cf	Pu (kW)	Energy (kWh)	Cost ($/kWh)
1	January	9.25	0.5078	15.23	11121	0.0272
2	February	9.25	0.5078	15.23	11121	0.0272
3	March	8.91	0.4879	14.64	10686	0.0284
4	April	8.35	0.4509	13.53	9875	0.0307
5	May	7.45	0.3829	11.49	8386	0.0361
6	June	5.64	0.2292	6.88	5021	0.0604
7	July	5.42	0.2100	6.30	4600	0.0659
8	August	4.29	0.1214	3.64	2659	0.1139
9	September	4.18	0.1135	3.41	2486	0.1219
10	October	6.54	0.3074	9.22	6732	0.0450
11	November	8.12	0.4349	13.05	9523	0.0318
12	December	9.48	0.5201	15.60	11389	0.0266
13	**AVERAGE**	**7.24**	**0.3562**	**10.68**	**7800**	**0.0513**

Table 5: Technical Specifications and Operating Parameters of the EWT DW54-500 Medium-Capacity Wind Turbine

	Month	c (m/s)	Cf	Pu (kW)	Energy (kWh)	Cost ($/kWh)
1	January	9.25	0.5643	282.13	205953	0.0168
2	February	9.25	0.5643	282.13	205953	0.0168
3	March	8.91	0.5423	271.15	197943	0.0175
4	April	8.35	0.5026	251.30	183447	0.0188
5	May	7.45	0.4310	215.52	157331	0.0220
6	June	5.64	0.2643	132.16	96480	0.0358
7	July	5.42	0.2425	121.26	88519	0.0390
8	August	4.29	0.1387	69.37	50641	0.0682
9	September	4.18	0.1293	64.65	47196	0.0732
10	October	6.54	0.3506	175.30	127968	0.0270
11	November	8.12	0.4856	242.81	177250	0.0195
12	December	9.48	0.5781	289.05	211007	0.0164
13	**AVERAGE**	**7.24**	**0.3995**	**199.74**	**145807**	**0.0309**

Table 6: Technical Specifications and Operating Parameters of the VESTAS V52 Medium-Capacity Wind Turbine

	Month	c (m/s)	Cf	Pu (kW)	Energy (kWh)	Cost ($/kWh)
1	January	9.25	0.3095	263.11	192074	0.0306
2	February	9.25	0.3095	263.11	192074	0.0306
3	March	8.91	0.2881	244.87	178753	0.0329
4	April	8.35	0.2518	214.06	156262	0.0376
5	May	7.45	0.1943	165.12	120540	0.0487
6	June	5.64	0.0920	78.20	57087	0.1029
7	July	5.42	0.0813	69.09	50439	0.1165
8	August	4.29	0.0368	31.32	22863	0.2569
9	September	4.18	0.0333	28.31	20666	0.2842
10	October	6.54	0.1400	118.98	86859	0.0676
11	November	8.12	0.2373	201.71	147248	0.0399
12	December	9.48	0.3237	275.10	200825	0.0292
13	**AVERAGE**	**7.24**	**0.1915**	**162.75**	**118807**	**0.0898**

3.4.2. Comparative Analysis of the Aerodynamic Performance of Wind Turbines (Cf and Pu)

An evaluation of the performance of the three wind turbine technologies (EWT DW54-500, Antaris 30 kW, and Vestas V52) reveals that a turbine's rated power does not necessarily determine its actual efficiency in a Sahelian context. The key factor lies in the match between the turbine's rated speed (Vn) and local wind conditions.

- The EWT DW54-500 model shows a remarkable match with the Iriba profile, displaying an average annual capacity factor (Cf) of 0.3995 (40%). Its strength lies in

its low rated speed (Vn = 10 m/s), which allows it to maximize energy conversion during Harmattan peaks (Cf = 0.5781 in December) while limiting the impact of the calm season in September (Cf = 0.1293). The average useful power (Pu) remains at a high level of 199.74 kW over the year.

- The Antaris 30 kW model, despite its low geometric power, demonstrates excellent technical consistency with an average annual Cf of 0.3562. Its low start-up speed (Vd = 2.2 m/s) is a major structural advantage during the low-speed season (August–September), maintaining a residual Cf of 0.1135 in September, when other turbines shut down.
- The Vestas V52 model is performing critically below expectations, with an average annual Coef of 0.1915. Designed for high wind speeds (IEC Class I/II, Vn = 15 m/s), it spends most of the year in partial transient operation. In August and September, it approaches complete technical shutdown (Cf = 0.0333 in September), indicating that the rotor is spinning almost at no load.

In onshore wind engineering, a capacity factor greater than 30% characterizes a highly profitable project.

The optimal efficiency observed for the EWT (39.95%) is consistent with the findings of Djongyang et al., who demonstrated through their work on the evaluation of wind energy conversion systems in Cameroon and Chad that Class III turbines (designed for moderate winds) consistently achieve capacity factors 15 to 20% higher than Class I/II wind turbines in the Sahelian environment. This phenomenon is also supported by Abakar et al. in their modeling of small turbine performance in remote areas, confirming that machines with low start-up speeds (Vd = 2.5 m/s), such as the Antaris 30 kW, ensure the continuous service essential for off-grid water pumping applications during periods of low wind.

3.4.3. Analysis of Economic Viability and Unit Energy Cost (Cost)

The assessment of the unit cost of electricity (Cost in $/kWh), calculated over a 20-year life cycle, makes it possible to quantify the financial return generated by the technical performance of each machine:

- The EWT DW54-500 wind turbine, Thanks to its high energy productivity (145.807 kWh monthly average), best amortizes the present value of the cost (PVC). It generates the cheapest electricity in the panel with an average cost of 0.0309$/kWh, fluctuating steadily between 0.0164 $/kWh (December) and 0.0732 $/kWh (September).
- The Antaris 30 kW wind turbine offers an average unit cost of 0.0513/kWh. Although this cost logically increases in September (0.1219$/kWh) due to lower production, it remains perfectly viable for off-grid applications.
- The Vestas V52 wind turbine has an average cost of 0.0898$/kWh, but experienced a sharp spike in September, reaching 0.2842 $/kWh.

From a comparative analysis perspective, and looking beyond IRENA's global data [45] (which places the range for global onshore wind power between 0.03 and 0.06 $/kWh), our economic findings demonstrate strong local relevance when applied to Africa's energy realities. Ouédraogo et al.,[46] in their technical-economic analysis of renewable energy in sub-Saharan Africa, highlight that the average cost of electricity generated by diesel generator networks in rural or remote areas generally ranges between 0.25 and 0.55 $/kWh, due to the prohibitive logistical costs of fuel supply.

When comparing our results to the study by Ouédraogo et al., the implementation of the EWT DW54-500 (0.0309 $/kWh) reduces the cost per kWh in Iriba by nearly eightfold. Similarly, the Antaris 30 kW (0.0513 $/kWh) proves to be highly competitive. These results validate the assertion that the integration of suitable turbines constitutes the most viable solution for achieving an economically sustainable energy transition in Chad.

Conclusion

This study validates the suitability of the Rayleigh distribution model for characterizing the wind resource at Iriba, confirming sufficient energy potential to power critical water infrastructure. The analysis demonstrates that harnessing this local resource would enable the automation of water pumping, thereby meeting the region's domestic and pastoral needs. Economically, the technology's competitiveness is demonstrated by a minimum levelized cost of energy (LCOE) of 0.024 $/kW, supporting long-term viable rural electrification.

However, the seasonal variability observed between June and October requires strategic planning to mitigate the resource's intermittency. To optimize the site's energy security, two main recommendations are made:

- Hybrid systems: Integrating photovoltaic generators would offset the seasonal decline in wind speed, thereby ensuring a smoothed annual output.
- Structural optimization: The installation of turbines with a hub height of 50 m is recommended to capture more stable laminar flows and maximize energy yield.

Converting Iriba's wind potential into electrical energy therefore constitutes a robust technical and economic solution to strengthen the resilience of local communities in the face of the climatic constraints of northern Chad.

Declaration of competing interest

The authors declare that this study has in no way been funded by any company or institution. It is the personal contribution of the paper authors.

Author contribution

A. Fia Oung-zetna (Lead author): Managed the study design, supervised data collection, and performed data analysis.

B. Mahamat Alhafis Zenalabidine: Actively participated in data processing in collaboration with the lead author, Fia Oung-zetna.

C. Dr. Mohamed Ansoumane CAMARA.: Provided overall supervision of the study

D. Souleymane Soumah : Provided overall supervision of the study

E. Pr. Djongyang Noel: Provided overall supervision of the study in collaboration with Dr. Mohamed Ansoumane CAMARA.

Clinical Trial Declaration

Clinical Trial: NOT APPLICABLE

Consent to Publication Declaration

Consent to Publication Statement: not applicable

Ethics and Participation Consent Declarations

Ethics and Participation Consent Statements: not applicable

Data Availability: The data from this study can be obtained from the corresponding author upon request.

Funding: The authors received no financial support for the research, authorship, and/or publication of this article.

Bibliography

[1] O. Edenhofer, K. Seyboth, F. Creutzig, et S. Schlömer, « On the Sustainability of Renewable Energy Sources », *Annu. Rev. Environ. Resour.*, vol. 38, nº 1, p. 169-200, oct. 2013, **https://doi.org/10.1146/annurev-environ-051012-145344**

[2] T. Hussain et M. Ahmad, « DISCRETE INVERSE RAYLEIGH DISTRIBUTION. », *Pakistan Journal of Statistics*, vol. 30, nº 2, 2014, Accessed on: 23 mach 2026. [On line]. Available on: **https://doi.org/10.3390/axioms15020140**

[3] P. Singh *et al.*, « Application of Rayleigh distribution for micro-wind turbine prediction: A case study on wind energy potential in Gorakhpur district at 10m height », in *AIP Conference Proceedings*, AIP Publishing LLC, 2026, p. 080001. Accessed on: 23 mach 2026. [On line]. Available on: **https://pubs.aip.org/aip/acp/article-abstract/3398/1/080001/3379112**

[4] N. L. Ongaki, C. M. Maghanga, et J. Kerongo, « Evaluation of the Technical Wind Energy Potential of Kisii Region Based on the Weibull and Rayleigh Distribution Models », *Journal of Energy*, vol. 2021, p. 1-17, juin 2021, h**ttps://doi.org/10.3390/axioms1502014**

[5] M. Gökçek, A. Bayülken, et Ş. Bekdemir, « Investigation of wind characteristics and wind energy potential in Kirklareli, Turkey », *Renewable Energy*, vol. 32, nº 10, p. 1739-1752, 2007, Accessed on: 23 mach 2026. [On line]. Available on r: https://doi.org/10.1016/j.renene.2006.11.017

[6] A. Serban, L. S. Paraschiv, et S. Paraschiv, « Assessment of wind energy potential based on Weibull and Rayleigh distribution models », *Energy Reports*, vol. 6, p. 250-267, 2020, Accessed on: 11 may 2026. [On line]. Available on: https://doi.org/10.1016/j.egyr.2020.08.048

[7] D. K. Kaoga, N. Djongyang, S. Y. Doka, et D. Raidandi, « Assessment of wind energy potential for small scale water pumping systems in the north region of Cameroon », *International Journal of Basic and Applied Sciences*, vol. 3, nº 1, p. 38, 2014, Accessed on: 1 april 2024. [On line]. Available on: **https://doi.org/10.14419/0c9qv646**

[8] Seydou Ouedraogo, Komlan Lolo, Kodjo Attipou, Ayite Senah Akoda Ajavon, Sonnou Tiem, et Institut Universitaire de Technologie/Université Nazi BONI, « Assessment of Wind Potential in the Perspective of Water Pumping in Sahelian Area of Burkina Faso », *IJERT*, vol. V9, nº 03, p. IJERTV9IS030301, mach 2020, d**oi: 10.17577/IJERTV9IS030301**.

[9] D. K. Kaoga, R. Danwe, S. D. Yamigno, et N. Djongyang, « Performance analysis of methods for estimating Weibull parameters for wind speed distribution in the district of Maroua », *Journal of Fundamental and Applied Sciences*, vol. 6, nº 2, p. 153-174, 2014,

Accessed on: 1 april 2024. [On line]. Available on: https://www.ajol.info/index.php/jfas/article/view/120930

[10] D. H. Didane, N. Rosly, M. F. Zulkafli, et S. S. Shamsudin, « Evaluation of Wind Energy Potential as a Power Generation Source in Chad », *International Journal of Rotating Machinery*, vol. 2017, p. 1-10, 2017, doi: 10.1155/2017/3121875.

[11] D. K. Kidmo, B. Bogno, K. Deli, M. Aillerie, et B. P. Ngoussandou, « Economic assessment of WECS for water pumping systems in the North Region of Cameroon », *Renewable Energy and Environmental Sustainability*, vol. 6, p. 6, 2021, Accessed by: 19 mach 2024. [On line]. Available on: https://www.rees-journal.org/articles/rees/abs/2021/01/rees200016/rees200016.html

[12] G. Al Zohbi, P. Hendrick, et P. Bouillard, « Evaluation du potentiel d'énergie éolienne au Liban », *Journal of Renewable Energies*, vol. 17, nº 1, p. 83-96, 2014, Accessed on: 16 august 2024. [En ligne]. Disponible sur: https://revue.cder.dz/index.php/rer/article/view/425

[13] V. G. Gormo, D. K. Kidmo, B. P. Ngoussandou, B. Bogno, D. Raidandi, et M. Aillerie, « Wind power as an alternative to sustain the energy needs in Garoua and Guider, North Region of Cameroon », *Energy Reports*, vol. 7, p. 814-829, 2021, Accessed on: 1 april 2024. [On line]. Available on: https://www.sciencedirect.com/science/article/pii/S2352484721005229

[14] D. Todeschini, L. Fagiano, C. Micheli, et A. Cattano, « Control of a rigid wing pumping Airborne Wind Energy system in all operational phases », *Control Engineering Practice*, vol. 111, p. 104794, 2021, Accessed on: 19 mach 2024. [On line]. Available on: https://www.sciencedirect.com/science/article/pii/S096706612100071X

[15] T. Jard, « Analyse et contrôle des parcs éoliens flottants pour la maximisation de la puissance produite via la relocalisation des plateformes en temps réel », PhD Thesis, École de technilogie supérieure, 2023. Accessed on: 17 september 2024. [On line]. Available on: https://espace.etsmtl.ca/id/eprint/3270/

[16] D. K. Kidmo, B. Bogno, K. Deli, et D. Goron, « Seasonal Wind Characteristics and Prospects of Wind Energy Conversion Systems for Water Production in the Far North Region of Cameroon », *Smart Grid and Renewable Energy*, vol. 11, nº 9, Art. nº 9, sept. 2020, doi: 10.4236/sgre.2020.119009.

[17] B. Safari et J. Gasore, « A statistical investigation of wind characteristics and wind energy potential based on the Weibull and Rayleigh models in Rwanda », *Renewable energy*, vol. 35, nº 12, p. 2874-2880, 2010, Accessed on: 21 august 2024. [On line]. Available on: https://www.sciencedirect.com/science/article/pii/S0960148110001990

[18] P. T. Kapen, M. J. Gouajio, et D. Yemélé, « Analysis and efficient comparison of ten numerical methods in estimating Weibull parameters for wind energy potential: Application to the city of Bafoussam, Cameroon », *Renewable Energy*, vol. 159, p. 1188-1198, 2020, Accessed on: 12 mars 2024. [On line]. Available on: https://www.sciencedirect.com/science/article/pii/S0960148120308909

[19] A. Algieri, D. A. Zema, A. Nicotra, et S. M. Zimbone, « Potential energy exploitation in collective irrigation systems using pumps as turbines: A case study in Calabria (Southern Italy) », *Journal of Cleaner Production*, vol. 257, p. 120538, 2020, Accessed on: 12 mach 2024. [On line]. Available on: https://www.sciencedirect.com/science/article/pii/S0959652620305850

[20] M. A. M. Safari, N. Masseran, et M. H. A. Majid, « Wind energy potential assessment using Weibull distribution with various numerical estimation methods: a case study in Mersing and Port Dickson, Malaysia », *Theor Appl Climatol*, vol. 148, nº 3-4, p. 1085-1110, may 2022, doi: 10.1007/s00704-022-03990-0.

[21] C. Matthew, « The multiple benefits of current and potential energy efficiency policies: A Scottish islands case study », *Energy Policy*, vol. 187, p. 114032, 2024, Accessed on: 12 mars 2024. [On line]. Available on: https://www.sciencedirect.com/science/article/pii/S0301421524000521

[22] H. Song, J. Marshall, D. J. McGillicuddy, et H. Seo, « Impact of Current-Wind Interaction on Vertical Processes in the Southern Ocean », *JGR Oceans*, vol. 125, nº 4, p. e2020JC016046, avr. 2020, doi: 10.1029/2020JC016046.

[23] M. H. Soulouknga, D. K. Kaoga, N. Djongyang, et S. Y. Doka, « Comparaison du potentiel énergétique éolien des trois zones climatiques du Tchad », *Journal of Renewable Energies*, vol. 19, nº 1, p. 49-58, 2016, Accessed on: 15 february 2024. [On line]. Available on: https://revue.cder.dz/index.php/rer/article/view/547

[24] O. Ruhnau, L. Hirth, et A. Praktiknjo, « Heating with wind: Economics of heat pumps and variable renewables », *Energy Economics*, vol. 92, p. 104967, 2020, Accessed on: 19 mach 2024. [On line]. Available on: https://www.sciencedirect.com/science/article/pii/S0140988320303078

[25] M. Al-Addous, S. Al Hmidan, M. Jaradat, E. Alasis, et N. Barbana, « Potential and Feasibility Study of Hybrid Wind–Hydroelectric Power System with Water-Pumping Storage: Jordan as a Case Study », *Applied Sciences*, vol. 10, nº 9, p. 3332, 2020, Accessed on: 19 mach 2024. [On line]. Available on: https://www.mdpi.com/2076-3417/10/9/3332

[26] Z. Wang, G. Fang, X. Wen, Q. Tan, P. Zhang, et Z. Liu, « Coordinated operation of conventional hydropower plants as hybrid pumped storage hydropower with wind and photovoltaic plants », *Energy Conversion and Management*, vol. 277, p. 116654, 2023, Accessed on: 19 mach 2024. [On line]. Available on: https://www.sciencedirect.com/science/article/pii/S0196890422014327

[27] T. Nikolaou, G. S. Stavrakakis, et K. Tsamoudalis, « Modeling and optimal dimensioning of a pumped hydro energy storage system for the exploitation of the rejected wind energy in the non-interconnected electrical power system of the Crete island, Greece », *Energies*, vol. 13, nº 11, p. 2705, 2020, Accessed on: 19 mach 2024. [On line]. Available on: https://www.mdpi.com/1996-1073/13/11/2705

[28] R. H. Tonsie Djiela, P. Tiam Kapen, et G. Tchuen, « Wind energy of Cameroon by determining Weibull parameters: potential of a environmentally friendly energy », *Int. J. Environ. Sci. Technol.*, vol. 18, nº 8, p. 2251-2270, august 2021, doi: 10.1007/s13762-020-02962-z.

[29] M. K. Nediguina, M. A. Abdraman, M. Barka, et A. M. Tahir, « Electric Water Pumping Powered by a Wind Turbine in North East Chad », *World Journal of Applied Physics*, vol. 7, nº 2, p. 21-31, 2022, Accessed on: 19 mach 2024. [On line]. Available on: https://www.researchgate.net/profile/Mahamat-Nediguina/publication/366259859_Electric_Water_Pumping_Powered_by_a_Wind_Turbine_in_North_East_Chad/links/6399cf1ee42faa7e75bf56af/Electric-Water-Pumping-Powered-by-a-Wind-Turbine-in-North-East-Chad.pdf

[30] K. Ameur, « le pompage éolien », *Bulletin des énergies renouvelables-N*, 2002, Accessed on: 14 august 2024. [On line]. Available on: https://www.doc-developpement-durable.org/file/Energie/eolien/pompage/pompage_eolien_cder.pdf

[31] C. Mone, M. Hand, M. Bolinger, J. Rand, D. Heimiller, et J. Ho, « 2015 cost of wind energy review », 2017, Accessed on: 13 mach 2024. [On line]. available on: https://escholarship.org/content/qt7p62d9rt/qt7p62d9rt.pdf

[32] L. Neij, « Cost dynamics of wind power », *Energy*, vol. 24, nº 5, p. 375-389, 1999, Accessed on: 13 mach 2024. [On line]. available on: https://www.sciencedirect.com/science/article/pii/S0360544299000109

[33] M. I. Blanco, « The economics of wind energy », *Renewable and sustainable energy reviews*, vol. 13, nº 6-7, p. 1372-1382, 2009, Accessed on: 13 mach 2024. [On line]. available on: https://www.sciencedirect.com/science/article/pii/S1364032108001299

[34] C. A. Komolafe, D. Fadare, L. Oladeji, et A. Gbadamosi, « Evaluation of wind energy potential in omu aran, nigeria using weibull and rayleigh models », *Green and Low-Carbon Economy*, vol. 2, nº 2, p. 131-141, 2024, Accessed on: 11 mai 2026. [On lige]. available on: http://ojs.bonviewpress.com/index.php/GLCE/article/view/679

[35] J. K. Lundquist, K. K. DuVivier, D. Kaffine, et J. M. Tomaszewski, « Costs and consequences of wind turbine wake effects arising from uncoordinated wind energy development », *Nature Energy*, vol. 4, nº 1, p. 26-34, 2019, Accessed on: 13 mach 2024. [On line]. available on: https://www.nature.com/articles/s41560-018-0281-2

[36] M. Gökçek et M. S. Genç, « Evaluation of electricity generation and energy cost of wind energy conversion systems (WECSs) in Central Turkey », *Applied Energy*, vol. 86, nº 12, p. 2731-2739, 2009, Accessed on: 13 mach 2024. [En ligne]. available on: https://www.sciencedirect.com/science/article/pii/S0306261909001433

[37] N. L. Ongaki, C. M. Maghanga, et J. Kerongo, « Research Article Evaluation of the Technical Wind Energy Potential of Kisii Region Based on the Weibull and Rayleigh Distribution Models », 2021, Accessed on: 11 may 2026. [on line]. available on: https://www.academia.edu/download/82385340/6627509.pdf

[38] A. Arias-Rosales et G. Osorio-Gómez, « Wind turbine selection method based on the statistical analysis of nominal specifications for estimating the cost of energy », *Applied Energy*, vol. 228, p. 980-998, 2018, Accessed on: 13 march 2024. [on line]. available on: https://www.sciencedirect.com/science/article/pii/S0306261918309735

[39] M. H. Soulouknga, S. Y. Doka, N. Revanna, N. Djongyang, et T. C. Kofane, « Analysis of wind speed data and wind energy potential in Faya-Largeau, Chad, using Weibull distribution », *Renewable energy*, vol. 121, p. 1-8, 2018, Accessed on: 11 may 2026. [on line]. available on: https://www.sciencedirect.com/science/article/pii/S0960148118300028

[40] D. K. Kidmo, K. Deli, et B. Bogno, « Status of renewable energy in Cameroon », *Renewable energy and environmental sustainability*, vol. 6, p. 2, 2021, Accessed on: 11 may 2026. [on line]. available on: https://www.rees-journal.org/articles/rees/abs/2021/01/rees200017/rees200017.html

[41] T. Wang, M. Umar, M. Li, et S. Shan, « Green finance and clean taxes are the ways to curb carbon emissions: An OECD experience », *Energy Economics*, vol. 124, p. 106842, 2023, Accessed on: 11 may 2026. [on line]. available on: https://www.sciencedirect.com/science/article/pii/S0140988323003407

[42] M. H. Ouahabi, H. Elkhachine, F. Benabdelouahab, et A. Khamlichi, « Comparative study of five different methods of adjustment by the Weibull model to determine the most accurate method of analyzing annual variations of wind energy in Tetouan-Morocco. », *Procedia Manufacturing*, vol. 46, p. 698-707, 2020, Accessed on: 11 may 2026. [on line]. available on: https://doi.org/10.1016/j.promfg.2020.03.099

[43] R. Berahab, « Energies renouvelables en Afrique: Enjeux, défis et opportunités », *Policy Center for the New South: Rabat, Morocco*, 2019, Accessed on: 13 february 2026. [On line]. available on: https://www.policycenter.ma/sites/default/files/PP%20-%2019-06%20(Rim%20Berahab).pdf

[44] DN, Moriasi, Gitau, MW, Pai, N., & Daggupati, P. (2015). « Modèles hydrologiques et de qualité de l'eau : mesures de performance et critères d'évaluation ». *Transactions of the ASABE* , *58* (6), 1763-1785.https://doi. 10.13031/trans.58.10715

[45] Müller, F. (2017). L'IRENA en tant qu'acteur glocal : voies vers une gouvernementalité énergétique. *Innovation : The European Journal of Social Science Research* , *30* (3), 306-322.. https://doi.org/10.1080/13511610.2017.1279538

[46] O. M., Dembélé, Y. et Somé, L. (2010). « Perceptions et stratégies d'adaptation aux changements des prélèvements : cas des paysans du Burkina Faso ». *Sécheresse* , *21* (2), 87-96, Accessed on: 11 may 2026. https://doi.10.1684/sec.2010.0244